CrystEngComm

Dynamic Article Links ►

Cite this: DOI: 10.1039/c0xx00000x

www.rsc.org/xxxxxx

ARTICLE TYPE

Epitaxial growth of (0001) oriented porous GaN layers by chemical vapour deposition

Oleksandr V. Bilousov,[a] Joan J. Carvajal,*[a] Oscar Martínez,[b] Juan Jiménez,[b] Hugh Geaney,[c,d] Francesc Díaz,[a] Magdalena Aguiló,[a] Colm O'Dwyer[c,d]

Received (in XXX, XXX) Xth XXXXXXXXX 20XX, Accepted Xth XXXXXXXXX 20XX

DOI: 10.1039/b000000x

LEDs with enhanced light extraction efficiency and sensors with improved sensitivity have been developed using porous semiconductors. Here, the growth of porous GaN epitaxial layers oriented along the [0001] crystallographic direction on Al_2O_3, SiC, AlN and GaN substrates is demonstrated. Lattice mismatch between the substrate and the porous GaN layer directly affects the structure and porosity of the porous GaN layer on each substrate. Deposition of unintentionally doped *n*-type porous GaN on non-porous *p*-type GaN layers allow for the fabrication of high quality rectifying *p-n* junctions, with potential application in high brightness unencapsulated GaN-based light emitting diodes and in high surface area wide bandgap sensor devices.

Introduction

III-N semiconductors, such as GaN, have a wide range of applications principally due to its wide direct band gap, being the most used materials for solid state lighting, both as LEDs and laser diodes , with emission in the UV and visible spectral ranges, being essential for the production of white light.[1] They present also interest for high temperature/high power electronics because of their large band gap, high thermal stability and excellent physical properties.[2]

In its porous form GaN is particularly interesting for developing optoelectronic devices with improved efficiency, such as LEDs with enhanced light extraction efficiency. This is due to the multiple reflections on the lateral walls of the pores and an "effective" reduced refractive index[3,4] that alleviates the high refraction index contrast between GaN, or other semiconductors, and air.[5,6] They are also interesting for their use in (bio)sensors, with improved sensitivity induced by the larger surface area of the porous structures.[7,8] Another attractive application of porous GaN is its use as a buffer layer to reduce the structural defects in non-porous GaN grown on foreign substrates, by reducing the stress due to the lattice mismatch.[9,10]

However, porous GaN has been typically fabricated by (photo)electrochemical and chemical etching methods.[11-13] These methods generally suffer from a lack of control over the size, morphology and distribution of the pores, making the fabrication of optoelectronic devices difficult. Furthermore, the use of these techniques might induce unwanted interface states and surface contamination and defects that can affect properties of the crystals, negatively affecting the performance of the systems based on them. Also, one has to take into account that anodization processes, to generate the required porosity, demand complex equipment for their control, and in general many of the electrolytes are highly toxic and/or corrosive. In the specific case of porous GaN, the ability to form relatively uniform, crystalline porous GaN layers over large areas through complex etching processes without photolithographic masking is challenging.[11,14] We have previously shown that it is possible to produce nanoporous GaN microparticles in a simple chemical vapor deposition (CVD) reactor,[15] without the need of additional etching or chemical treatments after growth for generating the porosity. The porosity in these particles is only present on the (0001) face. Recently, we demonstrated that these nanoporous GaN particles can be also grown on silicon substrates using a metallic catalyst, obtaining porous particles with a low density of defects.[16,17] However, the result is a polycrystalline porous GaN film with dual porosity (intraparticle and interparticle), where the porous particles, are not crystallographically oriented. In spite of this, electronically, GaN retains a clean surface with low presence of deep levels,[18] which is useful for applications requiring a high surface-to-volume ratio.

Here we show the possibilities of growing grains oriented along the [0001] crystallographic direction, so that all the pores would be aligned along the same direction through the directional effect provided by the substrate on which porous GaN is grown. The substrates for the oriented growth of nanoporous GaN were sapphire (which is the most widely used substrate for GaN deposition), SiC (also one of the most used substrates for GaN production), and commercial AlN and GaN epitaxial layers, since they have the same crystallographic structure and thus induce reduced lattice mismatches. The obtained porous films are characterized morphologically, structurally, electrically and optically. When growing on *p*-type non-porous GaN films, a clear *p-n* junction response was obtained, demonstrating the potential for functional devices based on epitaxial GaN and CVD grown porous GaN multilayers.

Materials and Methods

Nanoporous GaN thin layers were grown on different substrates by the direct reaction of metallic Ga with ammonia in a tubular CVD reactor, using gallium metal (99.999%) and ammonia (99.99%), as Ga and N sources, respectively. Metallic Ga was introduced into the system in the form of droplets in a quartz crucible.

The substrates used were Al_2O_3 (0001) (MTI Corporation), SiC (0001) (MTI Corporation), and AlN (0001) (Crystal IS, Inc.) and GaN (0001) thin films grown on sapphire (0001) substrates (MTI Corporation). The substrate was placed 1.7 cm above the Ga source. No catalyst was used in this case, in contrast when nanoporous GaN polycrystalline films were obtained on Si substrates by the same method;[17] therefore, the reaction was self-catalyzed.

The quartz tube of the furnace was degassed to a vacuum pressure of 1×10^{-2} Torr. Ammonia was then introduced through a mass-flow controller at a flow rate of 75 sccm, while the pressure was set at 15 Torr and the furnace was heated up to the reaction temperature of 1203 K. Then, the furnace was kept at constant temperature for 60 min under constant NH_3 flow and pressure, while the chemical reaction took place. When the reaction was finished, the furnace was cooled down to room temperature while the ammonia flow was stopped, thus the pressure of the system dropped to 1×10^{-2} Torr.

The nanoporous GaN layers deposited on the different substrates were characterized using a JEOL JSM 6400 scanning electron microscope (SEM).

The (0001) surface morphology of the porous films was visualized by Atomic Force Microscopy (AFM) using an Agilent 5500 microscope in the tapping mode, using Si tips with a diameter of 10 nm and oscillating at a resonance frequency of 75 kHz.

Rocking curves of the thin films were recorded using a Bruker-AXS D8-Discover diffractometer equipped with parallel incident beam (Göbel mirror), vertical θ-θ goniometer, XYZ motorized stage and a General Area Diffraction Detection System (GADDS). Samples were placed directly on the sample holder and the area of interest was selected with the aid of a video-laser focusing system. The X-ray diffractometer was operated at 40 kV and 40 mA to generate Cu Kα radiation. The GADDS detector was a HI-STAR (multiwire proportional counter of 30 × 30 cm with a 1024 × 1024 pixel). The rocking curves covered an omega angle of 6º from 120 frames, and were recorded at a step size of 0.05º and 15 s of exposition time per frame.

Two-probe electrical measurements of porous GaN samples were conducted using In/Ga liquid eutectic contacts and a Biologic SP-50 potentiostat. An In/Ga eutectic droplet was used as the Ohmic contact. Linear voltage sweeps were obtained between the range of -3 V and 3 V with a 50 mV/s sweep rate.

Cathodoluminescence (CL) imaging and spectra (at both room temperature and 80 K) and EBIC measurements at RT were carried out in a field emission scanning electron microscope (Carl Zeiss-LEO 1500) operating at 10 kV. For CL measurements, a XiCLOne mono-CL2 system from Gatan was used, the detection being done with a charge-coupled device camera.

For EBIC measurements, the electrical current generated by the electron beam was collected and amplified by a low noise current amplifier (MODEL DLPCA-200, FEMTO Messtechnik, Germany). These measurements conditions allowed spatial resolutions of the order of few hundred nanometers.

Results and discussion

Morphological characterization of the porous GaN films

Figure 1 shows the SEM top view images of the nanoporous GaN films obtained on the different substrates used in this work. Prior to the experiments, we expected porous GaN layers to grow oriented along the ***c***-crystallographic direction, since all our substrates belong to the hexagonal system and are oriented perpendicular to the [0001] direction. However, the morphology, grain structure and the crystallographic orientation of the films depends strongly on the lattice mismatch between the substrate and GaN.

We calculated the two-dimensional lattice mismatch from the expression to have an estimation of the biaxial stress of the samples:[19]

$$f_{(hkil)} = [(S^{L}_{(hkil)} - S^{S}_{(hkil)}) / S^{S}_{(hkil)}] \times 100 \qquad (1)$$

where $S^{S}_{(hkil)}$ and $S^{L}_{(hkil)}$ are the areas calculated from the periodicity vectors of the substrate and the layer, respectively, for the (0001) plane. Table 1 summarizes the lattice parameters used to calculate the lattice mismatch and the obtained values for the different substrates. The sign of the lattice mismatch indicates if the films are under either compressive or tensile strain when grown on a particular substrate. A negative lattice mismatch means that the plane of the substrate is larger than that of GaN, in this case the porous layer should be under tensile strain. A positive lattice mismatch means that the surface area of the (0001) plane of the substrate is smaller than that of GaN, thus the porous films suffer from compressive stress.

As it can be seen in Table 1, sapphire offers a negative lattice mismatch with GaN, while SiC and AlN result in positive lattice mismatch. The lattice mismatch calculated for the films grown on GaN is zero.[20,21] Thus, the porous GaN layer grown on sapphire should be compressed, whereas those layers obtained on SiC and AlN should be stretched. Furthermore, the absolute value of the lattice mismatch calculated for GaN/Al_2O_3 is larger than for GaN/SiC and GaN/AlN, and can be arranged in the following order from bigger to smaller: $f^{Al_2O_3}_{(0001)} > f^{SiC}_{(0001)} > f^{AlN}_{(0001)} > f^{GaN}_{(0001)}$.

Table 1. Lattice mismatch, calculated for the (0001) plane, between GaN and the different analyzed substrates

	Lattice parameters	Lattice mismatch, %
Substrate	*a* (Å)	$f_{(hkl)}$
Sapphire[22]	4.75	-14
6H-SiC[23]	3.07	7.7
AlN[24]	3.11	5.1
GaN[25]	3.19	0

Porous GaN obtained on Al_2O_3 appears in the form of a continuous layer of randomly oriented GaN particles, with porosity present on the (0001) face (see Figure 1a), as observed previously on Si and BN substrates.[16] In spite of such porosity, an ordered coverage of the surface of the substrate is apparent at low magnifications (see inset in Figure 1a).

In the case of SiC (0001), the smaller lattice mismatch and the similar thermal expansion coefficients with GaN, results in porous GaN growing as a quasi-continuous layer with porous GaN particles aligned along the [0001] crystallographic direction and pores on the (0001) GaN face (see Figure 1b). However, crystal grains do not tend to coalesce during growth, and individual particles are still evident in the image.

On AlN, a ***c***-oriented continuous quasi-porous GaN layer similar to that on SiC is obtained, but with a different morphology. Individual particles are not evident; however, the pores have and higher dispersion of shapes. Interparticle porosity in this case is favoured, while negligible intraparticle porosity (within each crystal) is found, as is the case for other growth regimes (see Figure 1c).[17]

Similar results to those obtained on AlN were obtained on GaN (0001) thin films on sapphire (see Figure 1d).

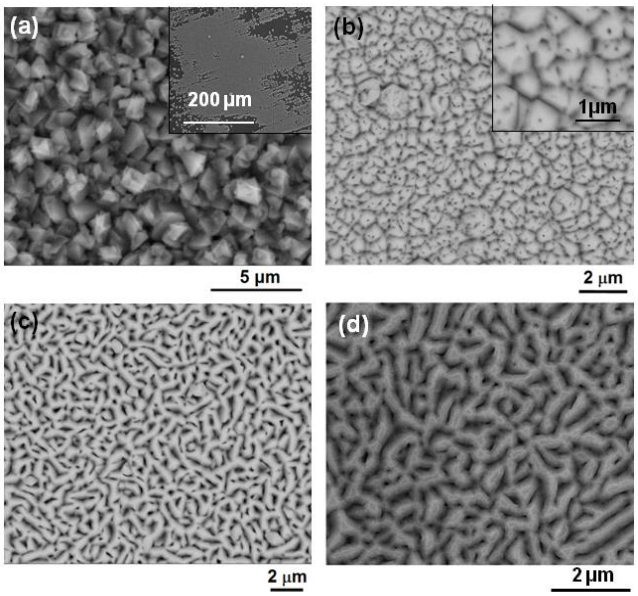

Figure 1. SEM images of porous GaN films obtained on (a) Al_2O_3 (0001), (b) SiC (0001), (c) AlN (0001) and (d) GaN (0001) thin films on sapphire.

The porous GaN epitaxial layers (grown via CVD) obtained on GaN (0001) coated sapphire (0001) substrates were further investigated to follow the evolution of the morphology of the pores and the growth rate with reaction times between 15 and 60 min. Figures 2(a-c) shows the top-down SEM images of porous GaN obtained. These micrographs show that by increasing the reaction times the diameters of the pores increases. The sample obtained at 15 min showed the highest degree of porosity, while the sample obtained after 60 min of reaction showed the lowest degree of porosity. This evolution of the pores with time seems to suggest that a coarsening of the pores is happening as the reaction time increases. Especially in the case of the CVD porous GaN obtained at 15 and 30 min, they have the appearance of a perfectly c-oriented continuous porous GaN layer, and the aspect of a true epitaxial porous layer. These results obtained on GaN (0001) coated sapphire (0001) substrates suggest that by decreasing the reaction time on the epitaxial growth of CVD porous GaN on AlN, also porous epitaxial layers would be obtained.

To know the thickness of the CVD porous GaN epitaxial layers obtained on GaN (0001) coated sapphire (0001) substrates, cross sectional-images of the samples were recorded by SEM, as shown in Figures 2(d-f), corresponding to 15, 30 and 60 min of reaction time, respectively. These cross-sectional micrographs clearly show the sapphire substrate, the non-porous GaN film with a thickness of ~5 µm, and the CVD porous GaN layer. The interface between the non-porous GaN film, and the CVD porous GaN layer are well defined and abrupt, which is the consequence of the change in density (material quantity) of the two layers. The thickness of the CVD porous GaN layer increases with reaction time, from ~0.5 µm at 15 min to 1.7 µm at 60 min.

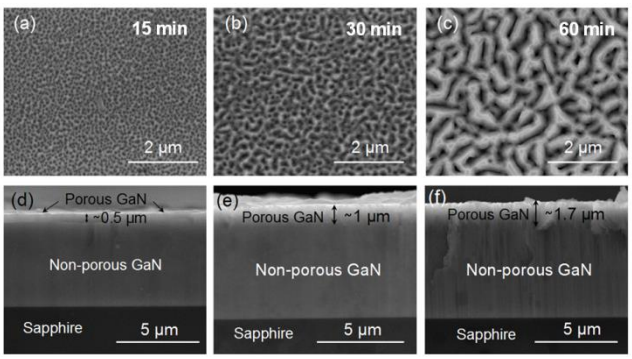

Figure 2. Top views and cross-sectional SEM images of the CVD porous GaN epitaxial layers obtained on GaN (0001) thin films coated sapphire (0001) substrates obtained after (a), (d) 15 min, (b), (e) 30 min, and (c), (f) 60 min reaction time.

AFM in tapping mode was used to visualize more in detail the CVD porous GaN layers, see Figure 3a. The porosity is evident in the image, and pores of different diameters are observed. Two profiles of the surface of the sample, corresponding to the lines indicated in Figure 3a, are shown in Figure 3b to describe the typical diameters of the pores, ranging from 200 to 300 nm.

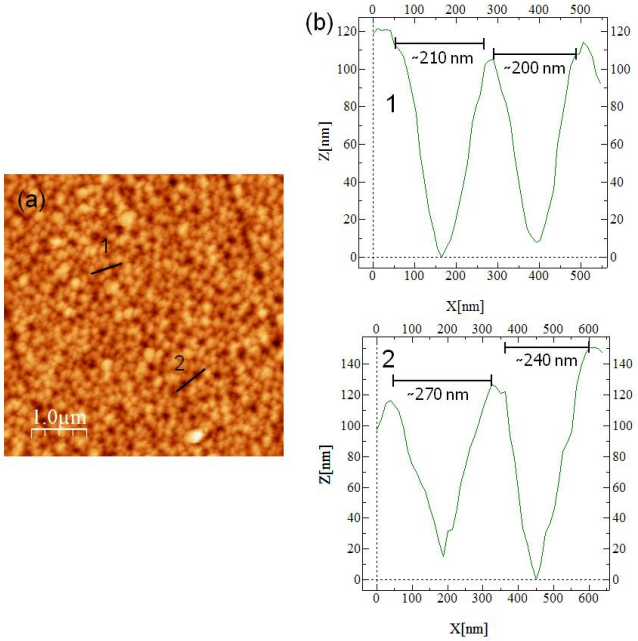

Figure 3. (a) AFM image and (b) profiles of the CVD porous GaN epitaxial layer grown for 30 min on non-porous GaN film coated sapphire (0001) substrates, taken at the locations highlighted in (a), showing the typical diameters of the pores.

Structural characterization of the CVD porous GaN epitaxial layer.

The rocking curves corresponding to the (0004) XRD reflection of both the CVD porous GaN epitaxial layer and the non-porous GaN film are shown in Figure 4. For the non-porous GaN film the measured FWHM is 0.428º, while for the CVD porous GaN epitaxial layer the FWHM is 0.419º. The reduction in the FWHM for the porous layer indicates the good structural quality of the epitaxial porous layer compared to epitaxially grown non-porous GaN films.

Furthermore, the rocking curve maximum is centered at 72.902º for the non-porous GaN film, as shown in Figure 3, while that of the CVD porous GaN epitaxial layer is centered at 73.082º. This shift indicates a slight relaxation of the porous layer. The reduction of the structural strain in the direction perpendicular to the plane of the sample can be determined by using the following expression:[26]

$$\Delta\epsilon_{\perp} = (c_{\text{strained}} - c_{\text{relaxed}})/c_{\text{relaxed}} \qquad (3)$$

were c_{strained} in our case accounts for the c parameter of the non-porous GaN grown on sapphire, and c_{relaxed} for the c parameter of the CVD porous GaN layer, calculated both from the analysis of the rocking curves. Accordingly, a reduction of the strain perpendicular to the (0001) plane of 0.21% can be estimated. This strain reduction stems from the benefit of internal porosity and the fact that the CVD porous GaN is grown on a native substrate, while the non-porous film is obtained on sapphire.

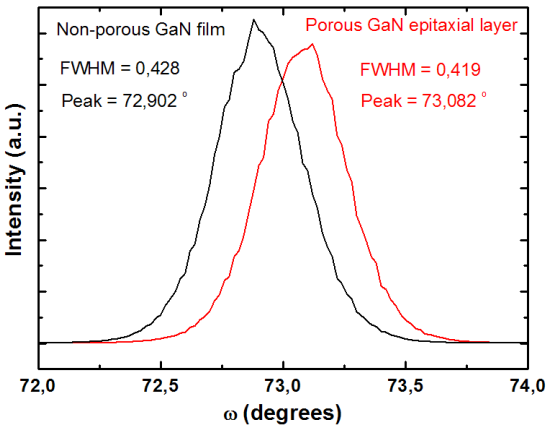

Figure 4. Rocking curves of porous GaN epitaxial layer grown on non-porous GaN films on sapphire.

Cathodoluminescence characterization.

Figure 5 shows SEM and corresponding panCL images recorded for the non-porous and CVD porous GaN films. The panCL image of the non-porous sample, Figure 5a, shows the typical granular luminescence emission pattern of GaN,[27] due to the high concentration of dislocations (>10^9 cm^{-2}) in these layers. In the corresponding SEM image, some porosity is apparent, likely related to the thermal treatment to which the substrate has been exposed during the growth process. The panCL image of the CVD porous sample, Figure 5b, shows a more uniform distribution of the luminescence. It is also important to note that the presence of the pores does not quench the luminescence arising from the porous GaN. In fact, when we compare this image with the corresponding SEM image, the pores (that can be clearly seen in the SEM image) are not visible in the CL image, with the exception of the larger pores, for which a dark contrast can be observed in the CL image.

Figure 5c shows the panCL image recorded at the border between the non-porous and the CVD porous GaN films. From this image it is clear that the extraction of light from the porous GaN is more efficient than from the non-porous film, related to the high quality of the CVD porous GaN epitaxial layer. Also, one can consider the beneficial effect of multiple reflections that the light generated by the sample suffers at the walls of the pores, which allows limiting the total reflection imposed by the refractive index contrast between GaN (2.29) [28] and air to be overcome. The CL spectra recorded in both regions are also shown in Figure 5c. The spectrum recorded for the non-porous film corresponds to the typical CL spectrum of a *p*-type GaN, with the donor-acceptor pair (DAP) luminescence located at 3.28 eV (378 nm), and a longitudinal optical (LO) phonon replica at 3.19 eV (388 nm). The spectrum recorded for the CVD porous GaN epitaxial layer exhibits the expected band-edge luminescence of *n*-type GaN, located at 3.40 eV (364 nm), with a FWHM of ~57 meV. Apart from this, a broad yellow luminescence (YL) band, normally attributed to point defects (Ga vacancies) and impurities such as oxygen and carbon[29] was also observed. For instance, in porous GaN deposited on Si by CVD, we observed the YL associated with a transition between the conduction band and a deep acceptor level, since its emission energy was independent of temperature.[30] In the present case, we

also observed an spatial variation in the intensity of the band-edge and YL bands, depending on the probed point along the sample. This can be attributed to different effects, such as an inhomogeneity in the distribution of impurities or defects in the GaN structure, but also to changes in the light extraction associated with the geometrical features of the pores.

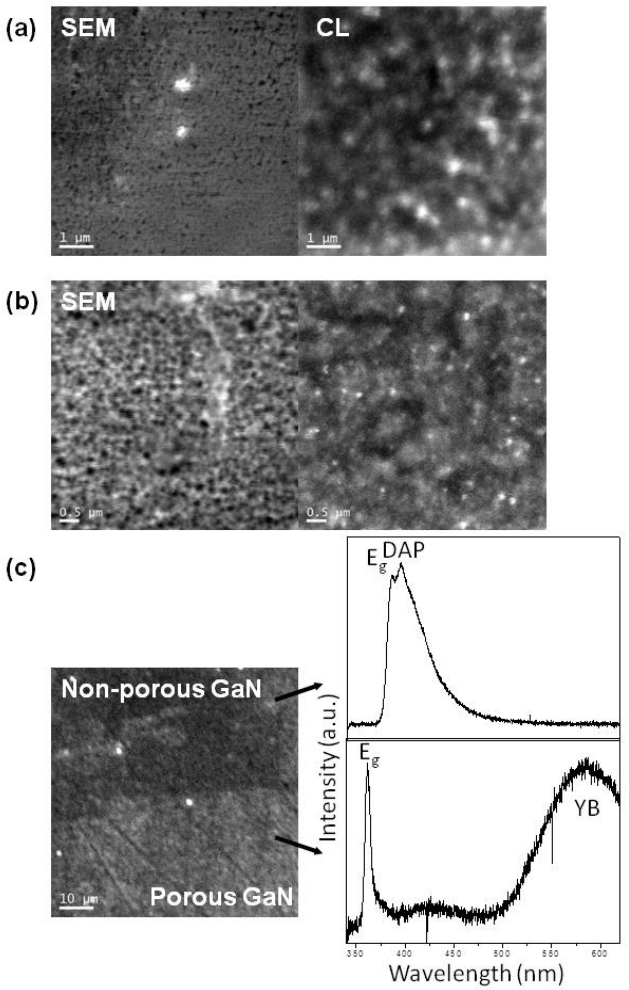

Figure 5. SEM and panchromatic CL images of (a) GaN on sapphire and (b) porous GaN. (c) Panchromatic CL image recorded at the border between porous and non-porous GaN, and CL spectra recorded at these two layers.

Electrical characterization

To further demonstrate the potential of the CVD porous GaN layers, we have grown them on a Mg-doped non-porous GaN film on sapphire. When such a structure is grown, a *p-n* junction is formed, as revealed by the non-linear I-V curve typical of a diode behaviour, as shown in Figure 6a. I-V curves were acquired between the underlying non-porous *p*-type GaN film and the porous GaN epitaxial layer. The clear *p-n* junction response confirms the formation of unintentionally doped *n*-type porous GaN. Microscopic examination (not shown here) confirms a clean interface without oxides or contaminants.

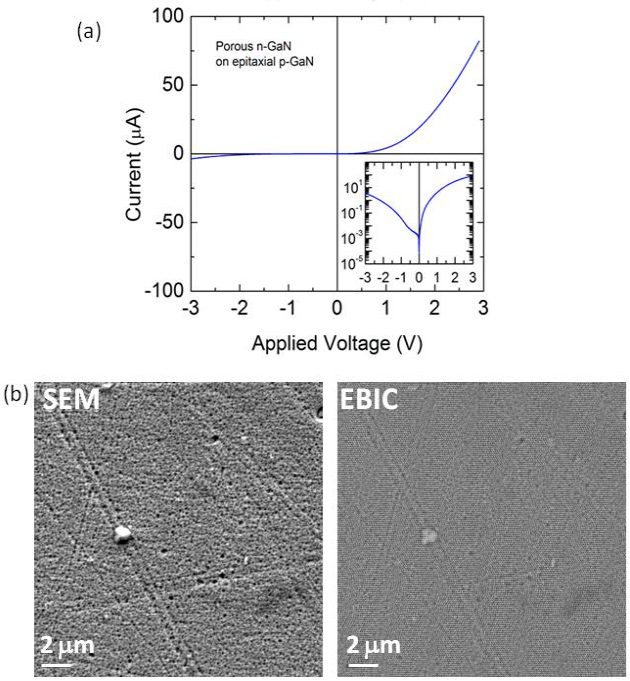

Figure 6. (a) I-V curve of the *p-n* junction formed from unintentionally doped CVD porous GaN epitaxial layers grown on non-porous *p*-type GaN films on sapphire. (b) SEM and (c) EBIC images of a CVD porous *n*-type GaN layer grown on a *p*-type non-porous GaN film on sapphire.

The high bias resistance turn-over of the porous *n*-type GaN occurs just above 1 V. At this voltage, high level carrier injection occurs across the *p-n* junction at higher applied bias, and is found to increase linearly with voltage above ~3V. [30,31] These values are consistent with the corresponding characteristic voltages found in uniform epitaxially grown GaN. In the case of CVD porous *n*-type GaN on non-porous *p*-type GaN films, current flow through the junction varies exponentially when the *p*-type material is positively biased. The turn-on (knee) voltage for the *p-n* junction is characteristically $\sim E_g/4q - E_g/2q$, i.e. 0.5 – 0.68 V. This response presents several features already observed in InN, GaN and other *p-n* juction nanowires arrays. Low reverse bias leakage currents are found for the porous assembly of GaN crystals in the layer. Assuming an abrupt, one-side junction by comparative analysis to coherent GaN films, the barrier potential V_B is estimated as $V_B = kT/q \ln(N_D N_A/n_i^2)$ = 0.72 V, where N_D = 10^{16} cm^{-3} and N_A = 10^{18} cm^{-3} are the donor and acceptor densities of the porous *n*-type GaN and the epitaxial *p*-type GaN of the *p-n* junction, respectively.

The measurements allow us to infer several important aspects for non-porous and CVD porous GaN interfaces and *p-n* junctions. Firstly, microscopic characterization has ruled out oxide or interfacial contaminants that would alter the effective barrier. From Figure 2, we can also conclude that the interface between the CVD porous and the non-porous GaN layers is well-defined and thus no significant tunnelling barrier exists either at the GaN-GaN interface or on the surface of the GaN with the Ohmic contact. Secondly, rectification arising from Schottky diodes contributions to transport are ruled out, since separate measurements[17] on the *n*-type GaN porous layer with In-Ga

contact (that includes considerations of the transport mechanism variations facilitated by intermetallic interfaces) and those from *p*-type GaN contacts including measurement with epitaxial *n*- and *p*-type layers, conclusively show Ohmic behaviour. The porous *p-n* junction here dominates the I-V curve response. Finally, measurements from several separate *p-n* junction tests exhibited similar I-V response.

In order to corroborate the satisfactory *p-n* junction behaviour of the CVD porous *n*-type GaN layer grown on a *p*-type non-porous GaN film on sapphire, EBIC measurements were also performed. Figure 6(b,c) shows the SEM and corresponding EBIC image of a region of the sample. No dark features are observed in the EBIC image, which means homogeneous carrier recombination. In particular, the pores do not act as traps for the charge carriers generated by the electron beam. Only some contrast could be observed for the bigger pores. This demonstrates the good performance of the formed *p-n* junction, proving the possibilities of the (0001)-oriented porous GaN layers obtained by CVD for the development of practical electrical and optoelectronic devices.

Conclusions

We have investigated the growth of porous GaN epitaxial layers on Al_2O_3, SiC, AlN and GaN substrates. The results show that the lattice mismatch between the substrate and the porous GaN layer plays an important role in achieving a continuous layer formed by discrete porous microparticles. The lattice mismatch was found to influence the degree of porosity. The undoped porous GaN epitaxial layer grown on non-porous GaN films on sapphire probed to be *n*-type. When grown on a non-porous *p*-type GaN layer, it allows for the fabrication of a *p-n* junction of excellent junction characteristics, with potential application in high brightness unencapsulated GaN-based light emitting diodes and in wide bandgap sensor devices.

Acknowledgments

This project was supported by the EU Framework 7 under Project No. FP7-SPA-2010-263044, the Spanish Government under Projects No. MAT2011-29255-C02-02, TEC2010-21574-C02-02, by the Catalan Authority under Project No. 2009SGR235 and by the "Conserjería de Educación de la Junta de Castilla y León" under Project No. VA166A11-2 . This work was also supported by the UCC Strategic Research Fund, and through the Irish Research Council New Foundations Award 2012. O.V. Bilousov is supported by Generalitat de Catalunya through the fellowship 2013FI-B2 00108.

Notes and references

[a] *Física i Cristal·lografia de Materials i Nanomaterials (FiCMA-FiCNA) and EMaS, Universitat Rovira i Virigli (URV), Marcel·lí Domingo s/n, E-43007 Spain*

[b] *GdS-Optronlab, Departamento Física Materia Condensada, Univ. de Valladolid, Edificio I+D, Paseo de Belén, 11, 47011, Valladolid, Spain*

[c] *Department of Chemistry, University College Cork, Cork, Ireland*

[d] *Micro & Nanoelectronics Centre, Tyndall National Institute, Lee Maltings, Cork, Ireland*

† Electronic Supplementary Information (ESI) available: [details of any supplementary information available should be included here]. See DOI: 10.1039/b000000x/

1 S. Nakamura and M. R. Krame,. *Proceedings of the IEEE*, 2013, **101 (10)**, 2211.
2 S. C. Jain, M. Willander, J. Narayan and R. Van Overstraeten, *Journal of Applied Physics*, 2000, **87**, 965.
3 C. O'Dwyer and C. M. Sotomayor Torres, *Front. Physics*, 2013, **1**, 18.
4. C. O'Dwyer, M. Szachowicz, G. Visimberga, V. Lavayen, S. B. Newcomb and C. M. Sotomayor Torres, *Nat. Nanotech.*, 2009, **4**, 239.
5 C. F. Lin, K. T. Chen, C. M. Lin and C. C. Yang, *IEEE Electron Device Lett.*, 2009, **30**, 1057.
6 M. H. Lo, P. M. Tu, C. H. Wang, C. W. Hung, S. C. Hsu, Y. J. Cheng, H. C. Kuo, H. W. Zan, S. C.Wang, C. Y. Chang and S. C. Huang, *Appl. Phys. Lett*., 2009, **95(4)**, 041109.
7 F. K. Yam and Z. Hassan, *Appl. Surf. Sci.* 2007, **253**, 9525.
8 A. Ramizy, Z. Hassan and K. Omar, *Sens. Actuators, B*, 2011, **155**, 699.
9 B. K. Ghosh, T. Tanikawa, A. Hashimoto, A. Yamamoto and Y. Ito, *J. Cryst. Growth*, 2003, **249**, 422.
10 M. Mynbaeva, N. Savkina, A. Tregubova, M. Scheglov, A. Lebedev, A. Zubrilov, A. Titkov, A. Kryganovski, K. Mynbaev, N. Seredova, D. Tsvetkov, S. Stepanov, A. Cherenkov, I. Kotousova and V.A. Dimitriev, *Materials Science Forum*, 2000, **338.**
11 D. J. Diaz, T. L. Williamson, I. Adesida, P. W.Bohn and R. J. Molnar, *J. Appl. Phys*., 2003, **94,** 7526.
12 B. Nie, B. K. Duan, P. W .Bohn, *ACS Appl. Mater. Interfaces*, 2013, **5(13)**, 6208.
13 L.-W. Jang, D.-W. Jeon, A. Y. Polyakov, H.-S. Cho, J.-H. Yun, D.-S. Jo, J.-W. Ju, J.-H. Baek and I.-H. Lee, *Applied Physics Express*, 2013, **6**, 061001.
14 J. A. Bardwell, I. G. Foulds, J. B. Webb, H. Tang, J. Fraser, S. Moisa and S. Rolfe, *J. Electron. Mater.*, 1999, **28**, L24-L26
15 J. J. Carvajal and J. C. Rojo, *Cryst. Growth Des.*, 2009, **9**, 320.
16 J. J. Carvajal, O. V. Bilousov, D. Drouin, M. Aguiló, F. Díaz and J. C. Rojo, *Microsc. Microanal*., 2012, **18**, 1.
17 O. V. Bilousov, J. J. Carvajal and D. Drouin, X. Mateos, F. Díaz and M. Aguiló and C. O'Dwyer, *ACS Appl. Mater. Interfaces*, 2012**, 4**, 6927.
18. S. S. Dhesi, C. B. Satgarescu and K. E. Smith, *Phys. Rev. B*,1997, **56**, 10271.
19 J. J. Carvajal, B. Raghothamachar, O. Silvestre, H. Chen, M. C. Pujol, V. Petrov, M. Dudley, M. Aguiló and F. Díaz, *Cryst Growth Des*,. 2009, **9,** 653.
20 H. Y. Wang, S. C. Huang, T. Y.Yan, J. R. Gong, T. Y. Lin and Y. F. Chen, *Materials Science and Engineering B*, 1999, **57**, 218.
21 C. Park, S. Yeo, J-ho Kim, D. Yoon and T. J. Anderson, *Thin Solid Films*, 2006, **498**, 94.
22 T. Huang, W. Parrish, N. Masciocchi and P. Wang, *Adv. X-ray Anal*. 1990, **33**, 295.
23. Shaffer Hannam, *J. Appl. Crystallogr*., 1969, **2**, 45.
24 H. Schulz, K. H. Thiemann, *Solid State Commun*., 1997, **23**, 815.
25 C. Balkas, C. Basceri and R. Davis, *Powder Diffraction*, 1995**, 10**, 266.
26 L. Görgens, O. Ambacher, M. Stutzmann, V. Miskys, F. Scholz and J. Off, *Appl. Phys. Lett.*, 2000, **78**, 577.
27 S. Dassonneville, S. A. Amorkane, B. Sieber, J. L. Farvacque, B. Beaumont and P. Gibart, *J. Appl. Phys.* 2001, **89**, 3736.
28 D. Brunner, H. Angerer, E. Bustarret, F. Freudenberg, R. Höpler, R. Dimitrov, O. Ambacher and M. Stutzmann, *J. Appl. Phys.*, 1997, **82**, 5090.
29 J. Neugebauer and C. G. Van de Walle, *Appl. Phys. Lett.*, 1996, **69**, 503.
30 J. O. Song, J. S. Ha and T. Y. Seong, *IEEE Electron. Dev. Lett.*, 2010, **57**, 42.
31 O. V. Bilousov, H. Geaney, J. J. Carvajal, V. Z. Zubialevich, P. J. Parbrook, A. Giguère, D. Drouin, F. Díaz, M. Aguiló and C. O'Dwyer, *Appl. Phys. Lett.*, 2013, **103**, 112103.